Ab initio potential-energy surface for the reaction Ca+HCl→CaCl+H

Gilles Verbockhaven
Institute of Theoretical Chemistry, Institute for Molecules and Materials (IMM), University of Nijmegen, Toernooiveld 1, 6525 ED Nijmegen, The Netherlands

Cristina Sanz
Institute of Theoretical Chemistry, Institute for Molecules and Materials (IMM), University of Nijmegen, Toernooiveld 1, 6525 ED Nijmegen, The Netherlands and Instituto de Matemáticas y Física Fundamental, Consejo Superior de Investigaciones Científicas (CSIC), Serrano 123, 28006 Madrid, Spain

Gerrit C. Groenenboom
Institute of Theoretical Chemistry, Institute for Molecules and Materials (IMM), University of Nijmegen, Toernooiveld 1, 6525 ED Nijmegen, The Netherlands

Octavio Roncero[a)]
Instituto de Matemáticas y Física Fundamental, Consejo Superior de Investigaciones Científicas (CSIC), Serrano 123, 28006 Madrid, Spain

Ad van der Avoird[b)]
Institute of Theoretical Chemistry, Institute for Molecules and Materials (IMM), University of Nijmegen, Toernooiveld 1, 6525 ED Nijmegen, The Netherlands

(Received 17 December 2004; accepted 8 March 2005; published online 23 May 2005)

The potential-energy surface of the ground electronic state of CaHCl has been obtained from 6400 *ab initio* points calculated at the multireference configuration-interaction level and represented by a global analytical fit. The Ca+HCl→CaCl+H reaction is endothermic by 5100 cm^{-1} with a barrier of 4470 cm^{-1} at bent geometry, taking the zero energy in the Ca+HCl asymptote. On both sides of this barrier are potential wells at linear geometries, a shallow one due to van der Waals interactions in the entrance channel, and a deep one attributed to the $H^-Ca^{++}Cl^-$ ionic configuration. The accuracy of the van der Waals well depth, $\approx$200 cm^{-1}, was checked by means of additional calculations at the coupled-cluster singles and doubles with perturbative triples level and it was concluded that previous empirical estimates are unrealistic. Also, the electric dipole function was calculated, analytically fitted in the regions of the two wells, and used to analyze the charge shifts along the reaction path. In the insertion well, 16 800 cm^{-1} deep, the electric dipole function confirmed the ionic structure of the HCaCl complex and served to estimate effective atomic charges. Finally, bound rovibrational levels were computed both in the van der Waals well and in the insertion well, and the infrared-absorption spectrum of the insertion complex was simulated in order to facilitate its detection. © *2005 American Institute of Physics*. [DOI: 10.1063/1.1899154]

I. INTRODUCTION

Chemical reactions involve a drastic change in the electronic structure from reactants to products. Harpoonlike reactions between metal atoms (M) and halide molecules (XR with X=F, Cl, Br, or I and R=H or CH_3) constitute nice examples of such reordering: one electron of the metal atom "jumps" towards the halide molecule and forms an unstable anion, which fragments and leads to products MX and R. The XR and MX systems are polar and possess strong electronic and vibrational transition dipole moments, so one may use the photon excitation of reactants and products to study the influence of electronic, vibrational, and rotational excitations of reactants, the final-state distribution of products, and the stereodynamics. In addition, the interaction between the reactants gives rise to van der Waals complexes that can be used to spectroscopically examine the transition state dynamics after the electronic excitation of the metal atom. A recent review by Mestdagh *et al.*[1] provides a comprehensive description of the reaction dynamics of these systems.

The harpoon mechanism was first studied for systems in which M is an alkali-metal atom.[2] These systems are relatively simple because the metal cation M^+ and the halogen anion X^- are both closed-shell systems, so that the first excited electronic state of the MX product (or rather M^+X^-, since it is ionic) is extremely high in energy and only the ground electronic state of the products is of interest. Many experimental studies on the reactive collisions of these systems have been performed.[1,2] The system studied mostly from a theoretical point of view is Li+HF (Ref. 3–8) because its number of electrons is relatively low, which allows accurate *ab initio* calculations. The experimental electronic spectra recorded for some of these systems, such as Na–HF (Ref. 9) and Li–HF,[10] have been nicely reproduced by theoretical calculations.[11–14] The bound levels in the excited electronic states decay through electronic predissociation. In the

[a)]Electronic mail: oroncero@imaff.cfmac.csic.es
[b)]Electronic mail: a.vanderavoird@theochem.ru.nl

case of Li–HF this process leads mainly to LiF products,[15] whereas for Na–HF it seems that only a negligible amount of NaF products is formed.[16,17]

The situation for alkali-earth atoms is far more complicated, because the M^+ cation is an open shell system in this case. The energy curves of the $M^+(^2S,^2D,^2P)+RX^-$ ionic states intersect with those of the $M(^1S,^1D,^1P)+RX$ covalent states, determining the regions where the electron jumps from the metal to the halide. The different crossings yield the *MX* product in particular states, $X\,^2\Sigma$, $A\,^2\Pi$, or $B^2\Sigma$. The excited *MX* products are chemiluminescent, and the analysis of their spectra provides information about the product state distribution and makes the experimental study of such reactions very attractive.

One of the best studied systems is Ca+HCl. The reaction $Ca+HCl\rightarrow CaCl+H$ is highly endothermic, and it has been studied with excited $Ca(^1D,^1P)$ atoms.[18–26] It was found[22] that when the excited Ca $4p$ orbital is aligned perpendicularly to the direction of approach to HCl the production of CaCl in the $A\,^2\Pi$ electronic state is enhanced, whereas a parallel alignment favors the production of CaCl in the $B\,^2\Sigma$ state. Such a correlation was explained by assuming that the p orbital of the excited Ca atom transforms into a CaCl molecular orbital.[22] The fact that the A/B branching ratio depends only weakly on the Ca p orbital alignment was attributed to the presence of a dominant channel towards the $CaCl(X\,^1\Sigma)$ ground state. Because some of the potential crossings seem to occur at long distances, they are mainly affected by the long-range behavior of the ionic and covalent potential surfaces. Models of such crossings qualitatively explain this A/B ratio dependence[27] and, moreover, lead to a quantitative understanding of the energy dependence of the $Ca(^1D)+HCl$ reactive cross sections.[28] However, these models are based on long-range interactions and introduce *ad hoc* parameters to fit the experimental results. *Ab initio* calculations of the multiple crossings are therefore necessary to get a deeper insight in these reactions.

An alternative experimental study on the reaction dynamics of this system has been made by photon excitation of the Ca atom in the $Ca(^1S)-HCl$ van der Waals complex.[29–32] In a covalent picture the excited states correlate to $Ca(^1D)$ and $Ca(^1P)$. For the case of $Ca(^1P)-HCl$, the electrostatic interaction yields one A' state with a linear equilibrium geometry, similar to the ground state of the complex, and two other states of A' and A'' symmetries with a T-shaped equilibrium geometry.[33] This situation explains the redshift and blueshift features of the Ca–HCl spectrum relative to the $Ca(^1P\leftarrow{}^1S)$ transition. The nonreactive electronic relaxation channels yielding $Ca(^1S,^1P)+HCl$ fragments are analyzed but were not observed. The dominant processes are either slow vibrational predissociation or electronic predissociation. The electronic predissociation is considered less probable since it is due to couplings between covalent states and those states do not intersect. By contrast, the ionic channels, associated with the formation of CaCl products, cross with the initially populated $Ca(^1D,^1P)-HCl$ covalent states, which explains why these channels become dominant. The CaCl product was initially not detected in its electronic ground (X) state either,[29–31] its detection being particularly difficult because of vibrationally cold $CaCl(X)$ produced in the process of formation of the van der Waals complex. Later, the vibrational state distribution of $CaCl(X,v)$ was observed[32] with a maximum as high as $v=30$ and extending up to $v=60$. This unusually excited vibrational distribution explains the difficulties in detecting $CaCl(X)$, and confirms that this fragmentation channel involving the ground adiabatic electronic state of the system is important.

Although the long-range interaction models applied to the ground as well as to the excited states[27,28,31,33] are partly based on *ab initio* data, there is no accurate *ab initio* calculation of the ground electronic state of CaHCl. The only available potential surface is based on a diatoms-in-molecules (DIMs) model[34] for collinear geometries. This model predicts a rather shallow HCaCl insertion well. This well is, however, much deeper in other related systems such as Ca–HF,[35] Mg–HF,[36] Sr–HF,[37] and Be–HF.[38] It is assumed that the well is artificially shallow in the DIM model because the contribution of the $H^-Ca^{2+}Cl^-$ configuration, among others, is not considered. This will be discussed below.

The aim of this work is the accurate *ab initio* calculation of the ground-state potential-energy surface, from Ca+HCl reactants to CaCl+H products, passing through the van der Waals and insertion wells. The first well is important in studying the photoinduced reaction dynamics for the excited states of Ca, while the second should be very important in determining the insertion mechanism in the reaction dynamics. The huge difference in well depth between the two wells introduces difficult problems in the *ab initio* calculations as well as in fitting the surface, as will be described below. The electronic properties of the states that produce the potential surface change along the reaction path because of multiple electron jump mechanisms. This will be analyzed by studying the electric dipole expectation value. Moreover, the dipole moment function allows the study of infrared transitions and the simulation of the spectrum obtained from the insertion well.

II. *AB INITIO* CALCULATIONS

The potential-energy surfaces were computed using the MOLPRO 2000 quantum chemistry package developed by Werner *et al.*[39] Two different methods were used. Ground and excited electronic states of the Ca atom and the full three-dimensional CaHCl ground-state potential surface for the chemical reaction were computed by the multireference configuration-interaction (MRCI) method with orbitals and a reference space obtained from complete active space self-consistent-field (CASSCF) calculations. The potential of the Ca–HCl van der Waals well in the entrance channel—the only channel involving two closed-shell entities—was also computed (for fixed H–Cl bond length) by the coupled-cluster method with single and double excitations and perturbative triples [CCSD(T)] and orbitals obtained from Hartree–Fock (HF) calculations. This method is most suitable for weak van der Waals interactions comprising predominantly dispersion forces.

Special attention was given to the choice of the atomic basis functions. In a recent paper, Leininger and Jeung[40] re-

TABLE I. Comparison of calculated excitation energies ΔE (in cm^{-1}) and oscillator strengths gf of the $^1P \leftarrow {}^1S$ and $^1D \leftarrow {}^1P$ transitions in Ca with experimental and literature data.

	^1P		^1D	
	ΔE	gf	ΔE	gf
Experiment[a]	23 652	1.79(3)	21 849	0.0051(14)
[b]	23 762	1.67[c]	22 576	0.006[c]
[d]	23 979		24 316	

[a]Excitation energies from Ref. 63, oscillator strengths from Refs. 64–66 for the $^1P \leftarrow {}^1S$ and $^1D \leftarrow {}^1P$ transitions, respectively.
[b]Reference 40.
[c]The gf values with the basis of Leininger and Jeung were computed by us.
[d]References 27,42.

ported the excitation energy of the $4s4p(^1P)$ and $3d4s(^1D)$ states of the Ca atom to show the quality of their calcium basis. The basis set is built on Wachters' $14s11p5d$ Gaussian-type orbital basis.[41] The $15s13p5d$ Gaussians were optimized on the $4s^2(^1S)$, $4s4p(^3P)$, and $3d4s(^3D)$ states. One diffuse s and one diffuse d orbital were added before the contraction into a $12s9p5d$ atomic basis, while two added f orbitals remain uncontracted. With this basis we performed MRCI calculations on the Ca atom including valence and core-valence correlations; the active space consisted of the $3s,3p,4s$, and $4p$ orbitals. The errors in the excitation energies of the ^1P and ^1D states are only about 100 and 750 cm^{-1}, respectively[40] (see Table I). This is smaller than the errors found with other bases, such as those reported by Meijer *et al.*[27,42] As reported in Table I, the $4s^2(^1S) \rightarrow 4s4p(^1P)$ oscillator strength agrees with experiment to within 10%. This justifies the choice of this basis for the present work. Once the basis for Ca was chosen, the Ca–HCl ground-state van der Waals minimum was computed with the MRCI method using different augmented correlation consistent basis sets for H and Cl. The results, listed in Table II, show that the binding energy of the Ca–HCl complex is converged with respect to the one-electron basis to within 1 cm^{-1} with the augmented correlation consistent polarized valence triple zeta[43] (aug-cc-pVTZ) and the augmented correlation consistent polarized valence quadruple zeta[44] (aug-cc-pVQZ) bases for H and Cl, respectively. These bases were chosen in all further calculations.

The global three-dimensional CaHCl potential-energy surface was computed using large scale internally contracted MRCI calculations with orbitals optimized by a CASSCF procedure. Core-core and core-valence correlations in the Ca atom were neglected in order to improve the stability of the CASSCF and MRCI procedures. In the CASSCF, as well as in the MRCI calculations the active set was restricted to the molecular orbitals correlating with the $3s$ and $3p$ orbitals of Cl, the $4s$ and $4p$ orbitals of Ca, and the $1s$ orbital of H. This choice was motivated by the mixing between the $4s^2$ and $4p^2$ configurations found for the Ca ground state: a ratio of 13 is to 1 is reported by Hansen *et al.*[45] Using this active space, 616 configuration state functions (CSFs) are included in the CASSCF calculations, while the MRCI is based on the same 616 reference configurations. For a more accurate description of the diatomic limits involved in the present work, one would need to open the Ca core (see below). In order to correct the MRCI energies for size inconsistency we applied the so-called Davidson (Q) correction.[46]

TABLE II. Van der Waals well depth D_e (in cm^{-1}, without CP correction) from MRCI calculations with different basis sets. The basis of Ref. 40 is used for Ca.

H\Cl	aug-cc-pVDZ	aug-cc-pVTZ	aug-cc-pVQZ	aug-cc-pV5Z
aug-cc-pVDZ	···	166.4	161.9	161.4
aug-cc-pVTZ	227.3	196.9	189.5	189.7
aug-cc-pVQZ	228.8	197.6	189.6	189.7
aug-cc-pV5Z	229.7	197.6	189.6	189.7

TABLE III. MRCI and CCSD(T) results for the equilibrium distance and depth D_e of the Ca-HCl van der Waals minimum, without and with CP correction.

		$D_e(cm^{-1})$	
Method	R_{HCl-Ca}(Å)	No CP	CP
MRCI	5.156	−189.5	−176.4
MRCI[a]	5.158	−187.2	−174.1
CCSD(T)	5.011	−229.5	−218.5

[a]From the global fit.

For the weakly bound Ca–HCl entrance channel complex the accuracy of the MRCI procedure was tested by performing CCSD(T) calculations with the same basis. Table III shows a comparison of the results. The Boys and Bernardi[47] counterpoise (CP) method was used to correct the Ca-HCl binding energy for the basis set superposition error (BSSE) in both MRCI and CCSD(T) calculations. The CP correction is the difference between the sum of the energies of the Ca and HCl monomers computed in the full Ca–HCl dimer basis and the sum of the monomer energies computed in the respective monomer bases. It was found that the maximum CP correction for $R_{Ca-HCl} \geqslant 4.5$ Å is on the order of 15 cm^{-1} for CCSD(T), as well as for MRCI. The binding energy of the weakly bound complex is reduced by about 5% by this correction. The definition of CP corrections for the product channel and especially in the reaction zone is not straightforward. Therefore, and because of the small size of the corrections found for the entrance channel, the CP correction was not applied in the calculations of the global potential surface.

The global potential was calculated on a grid of more than 6000 geometries that consists of three (overlapping) smaller grids, each described by a set of valence coordinates. Most points were computed on the grid with the valence coordinates given by the Ca–Cl bond length, the Cl–H bond length, and the Ca–Cl–H angle. The Ca–Cl bond length was varied from 4 to $12a_0$, the Cl–H bond length from 2.2 to $8a_0$, and the Ca–Cl–H angle from 0 to 180°, mostly in steps of 15°. The step size in the bond lengths was chosen smaller close to the equilibrium geometry. The other two grids on which supplementary points were generated were in H–Ca–Cl and Ca–H–Cl valence coordinates.

A separate grid of about 330 points was chosen for the MRCI and CCSD(T) calculations on the Ca–HCl entrance channel complex, i.e., in the region of the van der Waals

well. The H–Cl distance was frozen at its experimental equilibrium value of 1.2746 Å.[48] The Ca–Cl–H valence angle was varied between 0° and 180° in steps of 15° and the Ca–Cl distance ranged from 3.5 to $25a_0$. In total the energy was computed for about 6400 points.

It was mentioned above that the size of the active space in the CASSCF calculations and the number of the electrons that are explicitly correlated had to be restricted in order to ensure convergence of the CASSCF calculations. One of the reasons for the convergence problems is that the covalent and ionic potential surfaces have multiple crossings, responsible for the harpooning effect. When the covalent and ionic surfaces are very close to each other the CASSCF procedure may converge towards the higher surface and thus find a metastable solution, while a stable solution exists at lower energy. In addition, the CASSCF procedure sometimes converges to metastable solutions which do not have any physical meaning. In regions where such computational annoyances were observed both the covalent and ionic solutions were calculated. The orbitals were more or less forced to have the desired character by starting from a purely covalent or ionic initial guess. This was also a reason for making the three grids overlap; approaching a point from different directions sometimes produced different converged solutions. It was ensured that the results obtained in the end were always consistent, but it was sometimes difficult to obtain adequate initial guesses.

Although the calculations were performed on a grid described by three sets of valence coordinates we used Jacobi coordinates associated with the different reaction channels in dynamical calculations. The Ca+HCl reactant Jacobi vectors are the vector $\boldsymbol{R}_{\mathrm{HCl–Ca}}$ from the HCl center of mass to the Ca atom, and the vector $\boldsymbol{r}_{\mathrm{Cl–H}}$ from the Cl to the H nucleus. The lengths of these vectors are $R_{\mathrm{HCl–Ca}}$ and $r_{\mathrm{Cl–H}}$ and the Jacobi angle θ is the angle between them. The CaCl+H product Jacobi vectors $\boldsymbol{R}_{\mathrm{CaCl–H}}$ and $\boldsymbol{r}_{\mathrm{Cl–Ca}}$ are defined analogously, and the angle between these vectors is denoted by γ.

III. FITS AND CHARACTERISTICS OF THE POTENTIAL SURFACE

In order to use the potential-energy surface in dynamical calculations the *ab initio* points described above were fitted by analytical functions. Two fit procedures were applied: a fit to the complete set of 6400 points computed by MRCI on the global grid and a local fit in the region of the van der Waals well to the extra points calculated in the entrance channel. This local fit was applied both to the MRCI and CCSD(T) results and it was used to check the accuracy of the global fit in the weak-interaction region.

A. Global fit

We used a fit procedure developed by Aguado and co-workers,[7,49] but some modifications[50] were required. The original procedure starts from a many-body expansion of the potential of three interacting atoms A, B, and C

$$V_{ABC} = V^{(3)}(R_{AB},R_{AC},R_{BC}) + \sum_{A<B} V_{AB}^{(2)}(R_{AB}). \tag{1}$$

The sum of the atomic energies is first subtracted, the $V_{AB}^{(2)}$ are the pair energies, and $V_{ABC}^{(3)}$ is the three-body energy. The pair energies are expressed in terms of short and long-range contributions

$$V_{AB}^{(2)\mathrm{short}} = c_0^{AB}\frac{\exp(-\alpha_{AB}R_{AB})}{R_{AB}}$$
$$V_{AB}^{(2)\mathrm{long}} = \sum_{i=1}^{N} c_i^{AB}\rho_{AB}^i, \tag{2}$$

where $\rho_{AB}=R_{AB}\exp(-\beta_{AB}R_{AB})$ and N is the order of the polynomial in the long-range term. The three-body term is expressed as a polynomial of order M, the maximum of $i+j+k$, in the variables ρ_{AB}, ρ_{AC}, and ρ_{BC}

$$V^{(3)}(R_{AB},R_{AC},R_{BC}) = \sum_{i,j,k}^{M} d_{ijk}\rho_{AB}^i\rho_{AC}^j\rho_{BC}^k. \tag{3}$$

In the standard procedure the pair energies are first fitted to obtain diatomic potential curves of the form of Eq. (2), while the three-body contribution is found by subtracting the sum of the pair energies from the total interaction energy, and then fitted to Eq. (3). In the case of CaHCl this did not work well; the problem is related to the fact that each of the diatomic fragments shows an ionic/covalent crossing when the internuclear distance increases, which produces ionic/covalent crossings also in the global surface. Very high-order terms were needed in the fit of the three-body potential obtained after subtraction of the pair interactions and artificial oscillations appeared. Also, the usual procedure to represent curve crossings by diagonalizing a 2×2 matrix did not produce satisfactory fits, probably because multiple ionic states are involved (see below). So we used a modified version of the standard procedure in which the pair and three-body terms are fitted simultaneously and the pair terms have the form of the terms in the three-body energy with two of the exponents, i,j,k equal to zero. This implies that only the polynomial pair terms defined in Eq. (2) were included, but one should remember that these terms contain the variables ρ_{AB} that depend exponentially on the interatomic distances R_{AB}. Instead of a single three-body term we used two such terms, with different exponents $\beta_{AB}^{(L)}$, $\beta_{AC}^{(L)}$, and $\beta_{BC}^{(L)}$ in the variables $\rho_{AB}^{(L)}$, $\rho_{AC}^{(L)}$, and $\rho_{BC}^{(L)}$ with $L=1, 2$

$$V_{ABC} = \sum_{L=1}^{2} V_L^{(3)}(\rho_{AB}^{(L)},\rho_{AC}^{(L)},\rho_{BC}^{(L)}). \tag{4}$$

Each of the terms $V_L^{(3)}$ has the form of Eq. (3) with polynomials of order $N=8$ in the pair terms that have two of the indices i,j,k equal to zero and order $M=5$ in the real three-body terms. This gave a satisfactory representation of all the points on the global grid with no oscillations.

A feature of the potential that could not be reproduced with the original fitting procedure is the van der Waals well in the entrance channel. This minimum is about 80 times shallower than the global insertion minimum, which makes

TABLE IV. Root-mean-square deviation (rmsd, in cm^{-1}) of the global fit from the calculated MRCI *ab initio* points. The energy is relative to the Ca+HCl asymptote with HCl at its equilibrium distance; N_{geom} is the number of geometries within the given energy range.

Energy range	N_{geom}	rmsd
$E<100\,000$	6752	561
$50\,000<E<100\,000$	61	794
$25\,000<E<50\,000$	826	862
$10\,000<E<25\,000$	1965	663
$0<E<10\,000$	2818	429
$-10\,000<E<0$	838	299
$-17\,000<E<-10\,000$	243	266
$-200<E<100$	307	5

its representation very difficult. It has been shown[51,52] that the inclusion of extra three-body terms was useful to better describe the long range of the potential. The modified procedure applied here contains such terms and gives a good fit of the van der Waals well.

The root-mean-square error in the final fit is 561 cm^{-1}, but it is more illustrative to look at specific errors in different regions of the potential surface. These are listed in Table IV. The last row of this table shows the good quality of the global fit for the van der Waals well in the entrance channel. The major features of the surface are shown in the minimum-energy path in Fig. 1, the stationary points are given in Table V. Figure 2 shows contour plots of the global potential-energy surface for different values of the Ca–Cl–H angle chosen to illustrate the features near the stationary points listed in Table V. The full set of *ab initio* data and the code that generates the fitted potential can be obtained from the authors upon request.

In Table VI the dissociation limits of the global potential are compared with experimental data for the diatomic molecules to estimate the accuracy of the MRCI procedure. The difference between D_e computed from the fit and from the *ab initio* points is less than 6% for CaH, less than 2% for HCl, and about 1% for CaCl. Those values show that the fit in the regions close to the dissociation limits is accurate. Two dissociation energies are found to be overestimated (for HCl and CaH) and one is underestimated (for CaCl), which implies that the discrepancies cannot be explained by a systematic error in the description of the Ca or Cl atom. The equilibrium distances computed for CaCl and CaH are larger by

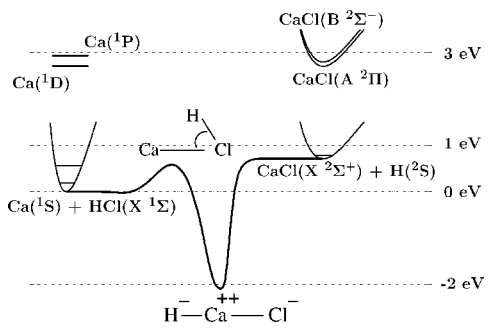

FIG. 1. Overview of the minimum-energy path for the Ca+HCl→CaCl +H reaction and the energies of relevant excited states.

TABLE V. Stationary points on the CaHCl ground-state potential-energy surface (distances in Å and energies in cm^{-1}). Valence coordinates are used in this table.

Stat. point	Coordinates			Energy
	R_{Ca-Cl}	R_{H-Cl}	H-Cl–Ca angle	
Reactants	∞	1.282	⋯	0
vdW minimum	5.194	1.268	0°	−187
Transition state	2.691	1.582	56°	4468
Global minimum	2.524	4.591	0°	−16 852
Products	2.500	∞	⋯	5101

0.06 Å than the experimental values, while the H-Cl bond length is reproduced very well. This overestimate of the bond length is a consequence of the fact that the core-core and core-valence correlations in the Ca atom were neglected in order to keep the CASSCF and MRCI procedures stable over the whole surface. Hansen *et al.*[45] have shown that the inclusion of core correlation leads to a contraction of the outer Ca orbitals, which would reduce the molecular bond lengths of CaH and CaCl.

The global minimum corresponds to a collinear geometry with the Ca atom inserted between H and Cl. The Ca–Cl and Ca–H distances obtained from the fit are 2.52 and 2.07 Å, respectively, slightly larger than the diatomic bond lengths in Table VI. From the *ab initio* points the minimum-

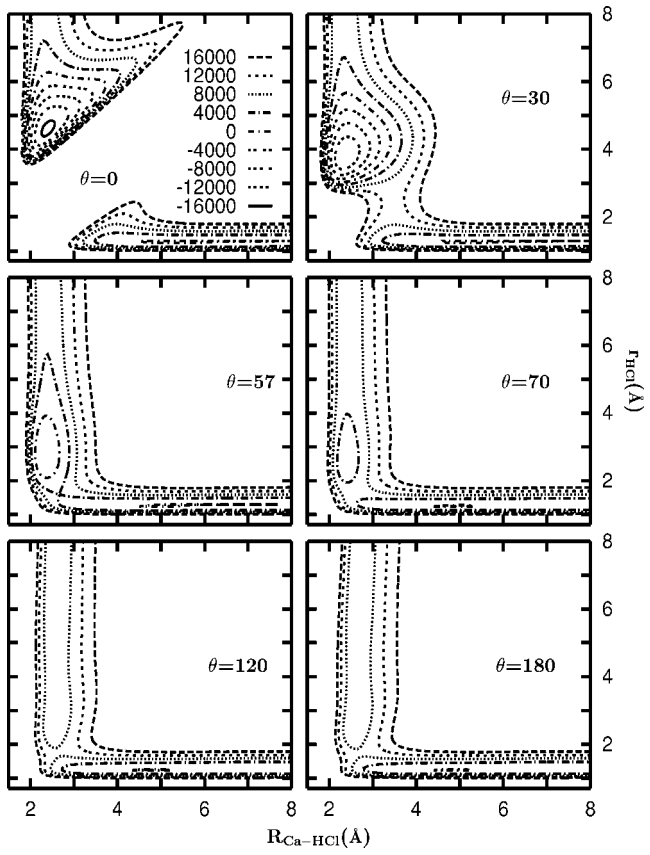

FIG. 2. Contour plots of cuts through the global potential-energy surface, as function of the Ca+HCl Jacobi coordinates. The contours are plotted for energy intervals of 4000 cm^{-1}, except for the cut at $\theta=57°$ where the contour at 4000 cm^{-1} was replaced by a contour at 4470 cm^{-1} in order to show the exact location of the transition state.

TABLE VI. Equilibrium distances R_e (in Å) and dissociation energies D_0 and D_e (in cm^{-1}) for the three diatomic limits of the CaHCl complex. Experimental data from Huber and Herzberg[48].

	R_e		D_e			D_0	
	This work	Expt.	This work	Theor.	Expt.	This work	Expt.
CaCl	2.500	2.439	32 835		32 990	32 650	32 988
CaH	2.065	2.002	15 175	14 428[a]	14 425	14 503	13 711[b]
HCl	1.282	1.275	37 936	37 193[c]		36 397	35 759

[a]Semiempirical estimate (Ref. 67).
[b]This number corresponds to an upper limit.
[c]Reference 68.

energy value is about $-16\,600\ cm^{-1}$ and the CaCl and CaH equilibrium distances are 2.59 and 2.12 Å, respectively. The difference in D_e between the fit and the *ab initio* points is only $200\ cm^{-1}$, less than 1.5%. The occurrence of this deep insertion well is due to the divalent character of the Ca atom. The outer occupied CASSCF molecular orbitals show important Ca(4*s*) contributions in this region and have dominant H or Cl character. We shall discuss this in more detail further on. Similar calculations performed on related systems such as Ca–HF,[35] Mg-HF,[36] Sr–HF,[37] and Be–HF (Ref. 38) also produced a deep insertion well.

The insertion well is accessed from the Ca+HCl entrance channel after surmounting a barrier. The saddle point is at a bent geometry with $\theta=57°$. Such a bent transition state is typical of these systems; it appears also for Ca–HF (Ref. 35) and Mg–HF (Ref. 36) and also in alkali–hydrogen halide systems such as Li–HF.[3,5,53] According to a DIM model for Li−H*X* systems[3] a resonance between two ionic structures, Li^+X^-H and Li^+H^-X, is responsible for such a bent transition state. This might be similar for systems containing alkali-earth atoms.

The H-Cl distance at the saddle point (1.58 Å) is considerably larger than in the free HCl molecule (1.28 Å). This was also observed in the other systems mentioned above. The origin of such a late barrier is an electron jump from Ca to HCl, forming HCl^-. Since HCl^- is repulsive, the H–Cl distance should increase in order to stabilize the Ca^+-HCl^- structure.

The saddle point is located at $4468\ cm^{-1}$ above the Ca+HCl limit. The effective barrier decreases when the HCl zero-point vibrational energy of $1540\ cm^{-1}$ is considered. The Ca+HCl→CaCl+H reaction is endothermic by $5101\ cm^{-1}$, which is more than the barrier height. The endothermicity is $3746\ cm^{-1}$ when zero-point energies are included.

B. van der Waals region

The shallow van der Waals well in the Ca–HCl entrance channel deserves careful examination. It is of great interest because the Ca–HCl complex is the precursor in the photoinitiated experiments of Soep and co-workers.[29–32] They assumed a linear Ca–HCl equilibrium configuration of the complex based on the geometries of known atom-HCl van der Waals complexes as Hg–HCl.[54] The present results, summarized in Table V, also predict such a linear equilibrium geometry with well depth $D_e=187\ cm^{-1}$ according to the global fit of the MRCI results.

The dissociation energy of the Ca–HCl complex was estimated to be much higher: $1200\pm400\ cm^{-1}$ by Menéndez *et al.*[55] It was determined from the maximum internal energy of the CaCl product observed in photoinitiated reactions, with the assumption that the product recoil energy is negligible. Later on, de Castro-Vitores *et al.*[23] reported an empirical potential with a binding energy of $980\ cm^{-1}$ at an equilibrium distance of 4.14 Å. This estimate of the binding energy assumed a contribution of van der Waals interactions plus an important charge-transfer contribution. The well depth based on van der Waals interactions alone was found to be $210\ cm^{-1}$, in fairly good agreement with the results reported in this work.

It was already mentioned above that in addition to the MRCI calculations CCSD(T) calculations were performed in order to check the accuracy of the potential in the van der Waals region. The CCSD(T) method, although not adequate for the whole surface because it is based on a single-configuration reference wave function, is more suitable than the MRCI method to compute the weak van der Waals interactions in the closed-shell Ca–HCl complex. The position and depth of the well obtained with the two methods are compared in Table III. The well depth from CCSD(T) calculations is about $40\ cm^{-1}$ larger than the MRCI value, i.e., about 20%, and the equilibrium distance R_e is about 3% smaller. The CP corrections for the BSSE, also shown in Table III, reduce D_e by about 5%. The best (CP-corrected) value is $D_e=218\ cm^{-1}$.

If there were an important charge-transfer contribution to this well depth, it would have emerged from the MRCI and CCSD(T) supermolecule calculations. We may therefore conclude that the experimental estimate of the dissociation energy by Menéndez *et al.*[55] is much too high, so their assumption that the product recoil energy in the experiment could be neglected is apparently not justified. The large discrepancy between the empirical estimate of de Castro-Vitores *et al.* and the present results originates from the charge-transfer contribution, which was probably overestimated in Ref. 23.

With HCl frozen at its equilibrium bond length a local fit of the potential in the van der Waals well region is performed both for the MRCI and CCSD(T) results. Since the CP correction cannot be applied to the MRCI results for the global

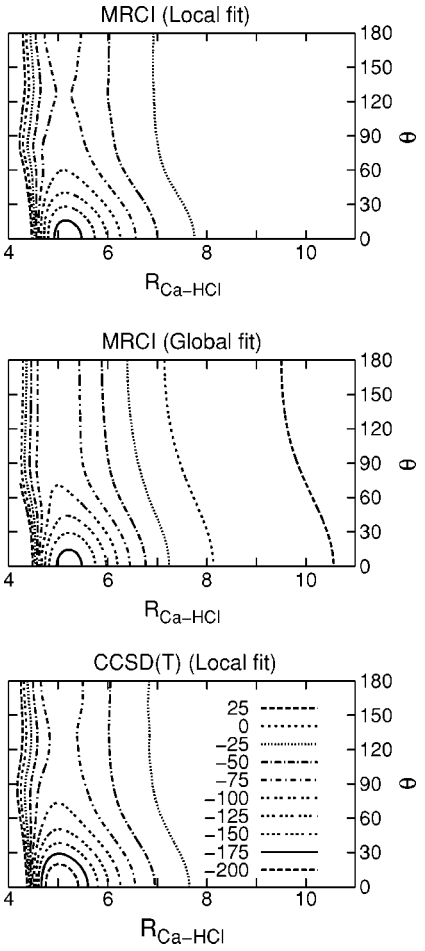

FIG. 3. Comparison between MRCI and CCSD(T) potentials for the entrance channel of the Ca+HCl reaction in the corresponding Jacobi coordinates. Energies in cm^{-1}, distance in Å, and angle θ in degrees.

potential we chose to use also the uncorrected MRCI and CCSD(T) data in the local fit of the van der Waals well. The interaction potential is written in the Ca–HCl Jacobi coordinates $R \equiv R_{\mathrm{HCl–Ca}}$ and θ and separated into long-range and short-range terms, which are expanded as

$$V_{\mathrm{short}} = \sum_{p=0}^{6} \sum_{l=0}^{9} d_{lp} R^p \exp(-\alpha R) P_l(\cos\theta), \tag{5}$$

$$V_{\mathrm{long}} = \sum_{n=6}^{14} \sum_{l=0}^{9} c_{ln} R^{-n} P_l(\cos\theta) \left[1 - \exp(-\beta R) \sum_{k=0}^{n} \frac{(\beta R)^k}{k!} \right],$$

where $P_l(\cos\theta)$ are Legendre polynomials. The coefficients c_{ln}, d_{lp}, and the nonlinear parameters α and β were fitted in a two-step procedure described in detail in Ref. 56. For the region of interest, i.e., $R \geq 4$ Å, the largest difference between the *ab initio* energies and the fitted values, 0.3 cm^{-1}, was found in the repulsive region, for $R=4$ Å and $\theta=30°$. For larger R values the energies are reproduced within 0.05 cm^{-1}.

The difference between the local fits performed on the CCSD(T) and MRCI data can be observed in Fig. 3, where they are also compared with the global fit. The global and local fits of the MRCI points agree very well (to within 2%),

TABLE VII. Bound levels (in cm^{-1}) in the Ca–HCl van der Waals well of the MRCI and CCSD(T) potentials for total angular momentum $J=0$.

v	MRCI	CCSD(T)
0	−111.38	−135.58
1	−90.46	−111.00
2	−71.96	−88.99
3	−65.46	−72.15
4	−55.64	−69.35
5	−49.30	−55.45
6	−41.45	−52.23
7	−35.28	−40.58
8	−29.81	−39.12
9	−28.68	−37.43
10	−23.39	−27.66
11	−19.22	−25.09
12	−14.03	−20.66
13	−12.41	−17.41
14	−10.30	−14.03
15	−6.74	−9.80
16	−3.69	−5.49
17	−0.13	−4.54
18		−2.41

which confirms the accuracy of the method developed by Aguado and co-workers[7,49] to reproduce even small wells in a global potential-energy surface.

A good test for comparing the two local fits obtained from the CCSD(T) and MRCI points was the calculation of the two-dimensional bound states in Ca–HCl Jacobi coordinates with the program TRIATOM.[57] The number of radial basis functions was 30 and the maximum j value in the angular basis was 20. The (variationally optimized) nonlinear parameters in the radial basis were $R_e=9.47$ and $9.74a_0$, $D_e=212$ and 190 cm^{-1}, and $\omega_e=6.8$ and 6.8 cm^{-1} for the CCSD(T) and MRCI potentials, respectively. The corresponding energy levels for total angular momentum $J=0$ are shown in Table VII. The dissociation energy D_0 is considerably smaller than the well depth D_e. Also, the difference in D_0 with the CCSD(T) and MRCI potentials, 24 cm^{-1}, is smaller than the difference in D_e, which is ≈ 40 cm^{-1}. The number of bound states with the two potentials differs only by one. The first excited state is the intermolecular stretch fundamental, and the second excited state has mostly bend character. The stretch and bend frequencies are not very different in the two potentials. This similarity shows that also the MRCI method, with a well-chosen basis, is able to describe the van der Waals region reasonably well. Combining this conclusion with the previous one, we may end this section by summarizing that the global CaHCl potential-energy surface obtained from the fit to the MRCI points gives a fairly good representation of the van der Waals well.

IV. ELECTRIC DIPOLE MOMENT

The electric dipole surface serves to study infrared, i.e., rovibrational, transitions within the ground electronic state that are of interest in this work. In addition, the electric dipole surface provides information about the electronic charge distribution in the complex, which is of great interest for

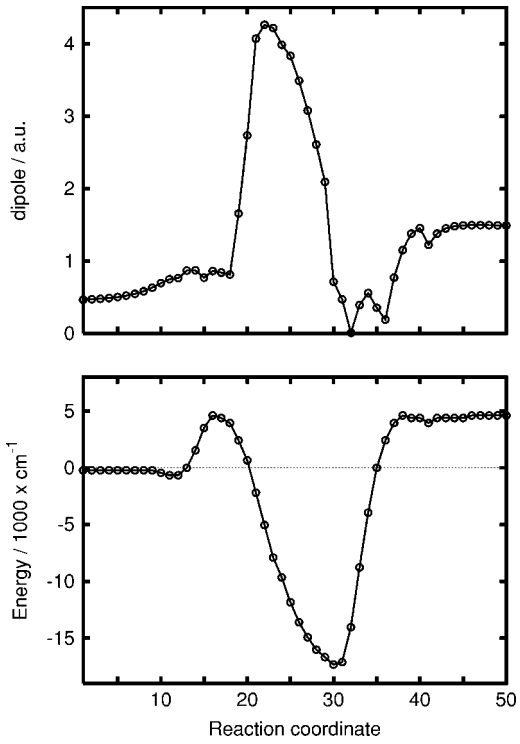

FIG. 4. Magnitude of the electric dipole (in a.u.) along the minimum-energy reaction path of CaHCl calculated at the MRCI level. The path length was computed from the distances between adjacent points, but contains an overall scale factor that is arbitrary.

harpoonlike reactions. Hence, the electric dipole moment expectation value over the MRCI wave functions was calculated in the regions of specific interest: along the minimum-energy reaction path, in the region of the Ca–HCl van der Waals well, and in the region of the HCaCl insertion well.

Figure 4 shows the dipole moment along the minimum-energy path from reactants to products. In the Ca+HCl and CaCl+H asymptotes it is very similar to the dipole of the HCl and CaCl fragments, respectively, which possess strong electric dipole moments. During the reaction the dipole shows some interesting variations. First, in the region of the saddle point it shows a maximum. Then, when the insertion minimum is approached there is a sudden decrease of the dipole and, subsequently, an increase when approaching the product region.

These variations of the dipole from the saddle point to the product region can be explained as follows. The increase of the dipole when approaching the saddle point is related to the ionic/covalent crossing. An electron jumps from Ca to HCl; the resulting bent $Ca^{+}HCl^{-}$ transition state complex has a large dipole moment. The much smaller dipole of the HCaCl insertion complex follows from the fact that the Ca atom in this complex is a doubly charged cation and that both the H and Cl atoms carry a single negative charge. The opposite dipole moments of the HCa and CaCl fragments in this $H^{-}Ca^{++}Cl^{-}$ complex very nearly cancel each other, which gives a very small net dipole moment. The electronic structure of HCaCl will be discussed below in more detail; it can be understood by first considering the CaCl molecule. The electronic structure of CaCl is well known:[58,59] CaCl consists essentially of an ionic $Ca^{++}Cl^{-}$ core with a diffuse electron around it. In HCaCl the highly polarizable electron around the $Ca^{++}Cl$ core is transferred to the H atom, thus producing a very stable ionic $H^{-}Ca^{++}Cl^{-}$ species. Finally, when the product region is approached, the H atom separates from CaCl and looses its negative charge, giving an increase of the dipole again.

In order to simulate the infrared spectrum of the HCaCl insertion complex, the dipole moment was calculated on a relatively dense grid of 520 points in this region, defined in the CaCl+H product Jacobi coordinates. The distance $R_{\mathrm{CaCl-H}}$ was varied from 4.4 to $20a_0$ in 13 steps, the bond length $r_{\mathrm{Ca-Cl}}$ from 4.369 to $7.369a_0$ in 8 steps, and the angle γ was given the values of 0°, 15°, 30°, 45°, 60°, and 90°. A frame is used with its origin at the center of mass of the complex, its z axis parallel to the Jacobi vector $\boldsymbol{R}_{\mathrm{CaCl-H}}$, and the Ca atom in the xz plane with $x>0$. The electric dipole surface in this region is represented by putting geometry-dependent point charges on the nuclei. The components of the dipole vector $\boldsymbol{d}$ can then be written as

$$
\begin{aligned}
d_x &= \frac{r_{\mathrm{Cl-Ca}} \sin\gamma}{m_{\mathrm{Ca}} + m_{\mathrm{Cl}}}[m_{\mathrm{Cl}}Q_{\mathrm{Ca}} - m_{\mathrm{Ca}}Q_{\mathrm{Cl}}], \\
d_z &= \frac{r_{\mathrm{Cl-Ca}} \cos\gamma}{m_{\mathrm{Ca}} + m_{\mathrm{Cl}}}[m_{\mathrm{Cl}}Q_{\mathrm{Ca}} - m_{\mathrm{Ca}}Q_{\mathrm{Cl}}] \\
&\quad + \frac{R_{\mathrm{CaCl-H}}}{M}[(m_{\mathrm{Ca}} + m_{\mathrm{Cl}})Q_{\mathrm{H}} - m_H Q_{\mathrm{Ca}} - m_H Q_{\mathrm{Cl}}],
\end{aligned}
\tag{6}
$$

where γ is the angle between the two Jacobi vectors, M is the total mass, and m_α and Q_α are the mass and effective charge of atom α. With the aid of Eq. (6) and the neutrality condition $Q_{\mathrm{H}}+Q_{\mathrm{Ca}}+Q_{\mathrm{Cl}}=0$ the effective atomic charges can be obtained from the calculated electric dipole moment.

The effective point charges were fitted to a series of products of Rydberg polynomials of the same form as the three-body terms in the potential [see Eq. (3)]. The root-mean-square errors in these fits were 0.09 and 0.15 D for the x and z components, respectively. Figure 5 shows the geometry dependence of the electric dipole vector obtained from the fit. In the same figure the fit of the *ab initio* computed dipole function is compared with a dipole function obtained with constant point charges $Q_{\mathrm{Ca}}=+\frac{4}{3}$, $Q_{\mathrm{Cl}}=-\frac{2}{3}$, and $Q_{\mathrm{H}}=-\frac{2}{3}$. In the region of the insertion well (marked with dashed contours in the figure) the agreement is very good. Hence, the assumption that the insertion well corresponds to an ionic complex $H^{-}Ca^{++}Cl^{-}$ holds to a large extent, although not completely. Figure 6, which shows the effective atomic charges in the region around the insertion well, confirms this picture.

Also, in the Ca–HCl van der Waals well the electric dipole was calculated and fitted. Reactant Jacobi vectors $\boldsymbol{R}_{\mathrm{HCl-Ca}}$ and $\boldsymbol{r}_{\mathrm{Cl-H}}$ were used in this case. The distance $R_{\mathrm{HCl-Ca}}$ was varied from 8 to $15a_0$ in 10 steps, the bond length $r_{\mathrm{H-Cl}}$ from 2.01 to $3.01a_0$ in 6 steps, and the angle γ was given the values of 0°, 15°, 30°, 45°, and 60°, which yields 300 points in total. The main contributions to the dipole function are the strong permanent dipole moment on HCl and the weaker one induced by its electric field on the Ca atom. The components of the dipole moment were fitted

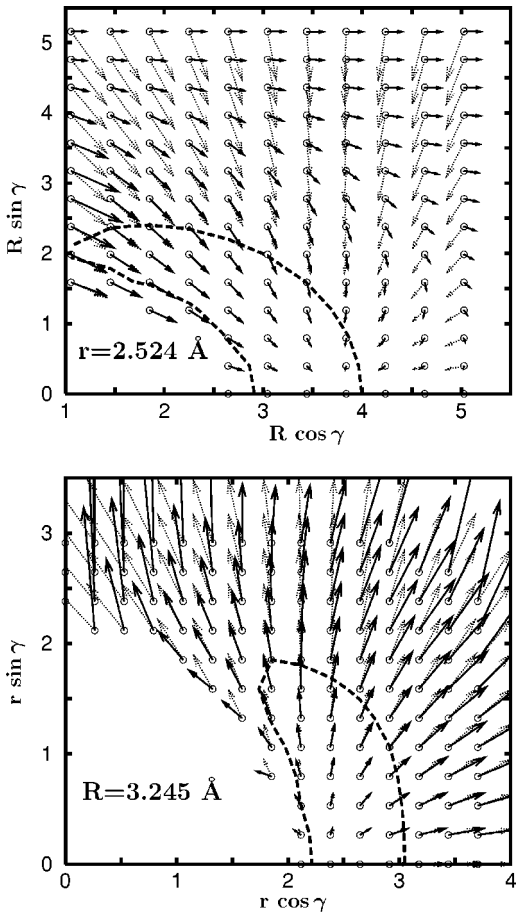

FIG. 5. Electric dipole vectors in the region of the HCaCl insertion well. Configurations where the potential energy is 7000 cm^{-1} above the bottom of the well are marked by a dashed contour. Top panel: for $r \equiv r_{\mathrm{Cl-Ca}}$ fixed at its equilibrium value of 2.524 Å with $R \equiv R_{\mathrm{CaCl-H}}$ and γ being CaCl+H product Jacobi coordinates. Bottom panel: for R fixed at its equilibrium value of 3.245 Å. The solid arrows indicate the dipole from the fit, the dotted arrows the constant effective charge model (see text).

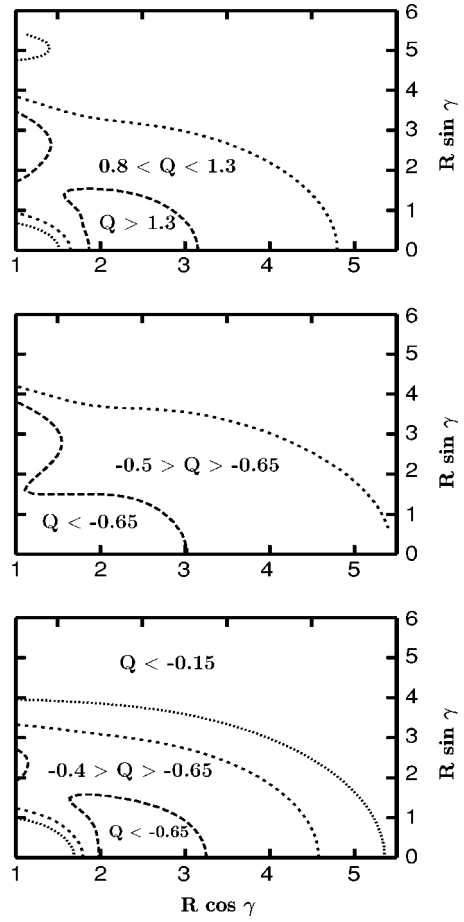

FIG. 6. Effective charges that fit the electric dipole moment [see Eq. (6)] in the region of the insertion well. Top panel: Q_{Ca}, middle panel: Q_{Cl}, and bottom panel: Q_{H}. The CaCl-H product Jacobi coordinates are the same as in Fig. 5.

with the same kind of formulas as the interaction energy in this region [cf. Eq. (5)]. Associated Legendre functions $P_{lm}(\theta)$ with $m=0$ were used for d_z and $m=1$ for d_x. The result is shown in Fig. 7, in a body-fixed frame in which the three atoms lie in the xz plane, with z parallel to $\boldsymbol{R}_{\mathrm{HCl-Ca}}$.

V. SPECTRUM OF THE INSERTION COMPLEX

The deep insertion well can be inspected by infrared spectroscopy; in this section we simulate the absorption spectrum of the insertion complex. Two different methods will be used for this purpose, and a body-fixed frame based on product Jacobi coordinates.

First, we used a grid method that is very efficient to compute excited states over a large range of energies, because it avoids an *a priori* choice of a basis set. Wave-packet simulations were performed on a three-dimensional grid of 256×128 equidistant points for the radial coordinates $R_{\mathrm{CaCl-H}}$ and $r_{\mathrm{Cl-Ca}}$, with $2 \leqslant R \leqslant 8$ Å and $2 \leqslant r \leqslant 5$ Å, and 50 Gauss–Legendre quadrature points for the angle γ. Wigner rotation matrices in terms of three Euler angles describe the overall rotation of the complex. Details of the method can be found in Ref. 60. In order to simulate infrared absorption by excitation from a particular rovibrational level Φ_n^J, the initial wave packet is constructed as $\Psi_{t=0} = \boldsymbol{d} \cdot \boldsymbol{e} \Phi_n^J$, where $\boldsymbol{d}$ is the dipole moment function and $\boldsymbol{e}$ is the electric polarization vector of the incident light. In order to simulate a particular $J \rightarrow J'$ rovibrational transition the initial wave packet is pro-

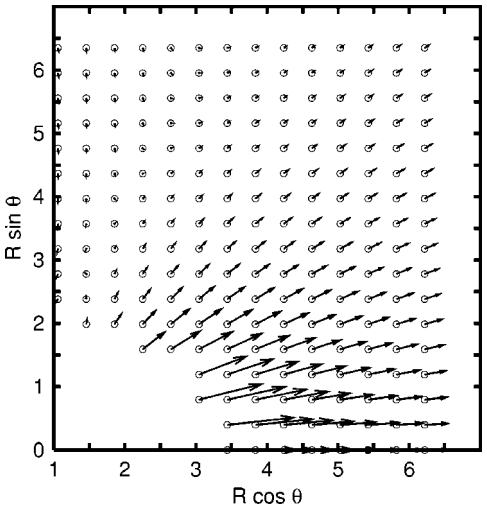

FIG. 7. Electric dipole vectors in the region of the van der Waals well. The HCl-Ca Jacobi coordinates are $R \equiv R_{\mathrm{HCl-Ca}}$ and θ, while $r_{\mathrm{H-Cl}}$ is fixed at its equilibrium value of 1.2746 Å.

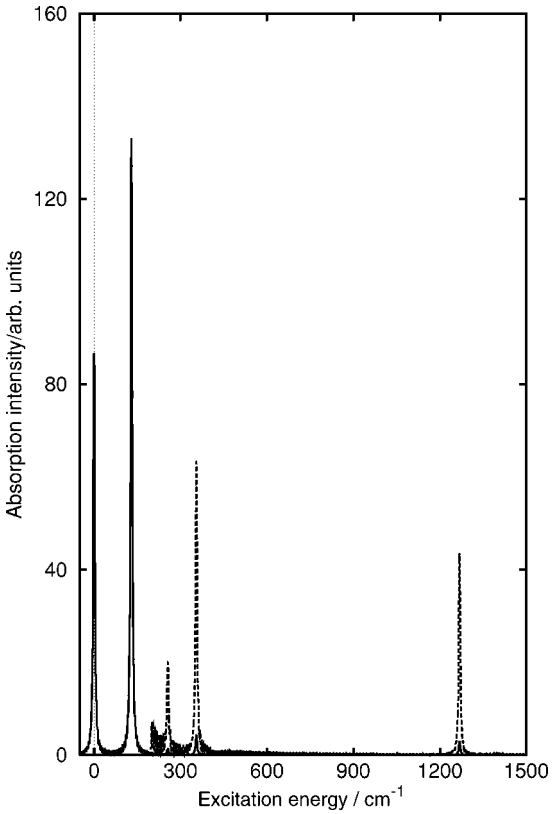

FIG. 8. Absorption spectrum of the HCaCl complex for $J=0\rightarrow 1$ transitions as a function of excitation energy simulated using the wave-packet method described in the text. The $J=0$ zero-point energy is 934.29 cm^{-1} with respect to the bottom of the well at $-16\,852$ cm^{-1}.

jected on the J' subspace[60] by the application of an operator $P_{J'}$ containing Wigner rotation matrices. The absorption spectrum as a function of energy E is then obtained from the Fourier transform of the autocorrelation function

$$\sigma(E) \propto \frac{1}{2\pi\hbar}\mathrm{Re}\int_0^\infty \exp(iEt\hbar)\langle\Psi_t|P_{J'}|\Psi_{t=0}\rangle dt = \sum_{n'} |a_{n'}|^2\delta(E-E_{n'}), \quad (7)$$

where $a_{n'}=\langle\Phi_{n'}^{J'}|P_{J'}|\Psi_{t=0}\rangle$, while $\Phi_{n'}^{J'}$ and $E_{n'}$ are the wave functions and energies of the vibrationally excited states n'. The evaluation of such an expression requires propagation up to $t=\infty$, in principle. In the present case the propagation was continued for 6 ps, in steps of 1 fs, to scan a large energy interval. Before the Fourier transform was performed the autocorrelation function was multiplied by an exponential damping function $\exp(\Gamma t/\hbar)$ with parameter $\Gamma=3$ cm^{-1}, so that the rhs of Eq. (7) transforms into a sum of Lorentzian functions of width Γ. This value of Γ is smaller than the energy separation of the excited states and all peaks in the spectrum are fully resolved.

Figure 8 shows the spectrum thus simulated for the transition from the ground vibrational state with $J=0$ towards all final states with $J'=1$, as a function of the excitation energy. The first peak at very low energy and not separately visible in Fig. 8 corresponds to a pure rotational transition to the ground level of $J'=1$, with Ω, the projection of the total angular momentum on the body-fixed z axis (the CaCl–H vector), equal to zero. The peak at 130 cm^{-1} corresponds to the fundamental bend excitation with $|\Omega|=1$; it demonstrates that perpendicular transitions are important. This state is a 50-50 mixture of basis functions with $\Omega=1$ and $\Omega=-1$ with definite parity under inversion of the spatial coordinates; it is nearly degenerate with a similar level of opposite parity. The weak peak at 259 cm^{-1} is the $\Omega=0$ component of the bend overtone, while the peaks at 358 and 1271 cm^{-1} correspond to the Ca–Cl and H–CaCl stretch motions, respectively.

There is no significant absorption intensity above 2000 cm^{-1}. Similar results were obtained for a few other initial vibrational states. This allows us to conclude that only bound states up to this energy are required, i.e., $\approx$30 states for $J=0$. The simulation of the spectrum corresponding to a Boltzmann distribution at nonzero temperature would require a series wave-packet calculations for each thermally occupied initial state Φ_n^J and final $J'=J-1,J,J+1$ according to the dipole selection rules. Such a procedure is advantageous only when very high excited vibrational states are involved. In the present case it was more convenient to calculate all relevant bound states directly.

The simulation of the infrared spectrum at different temperatures was performed by calculating all bound states up to 3000 cm^{-1} above the zero-point level, for J values up to 10, inclusive. The method used is described in Ref. 14. The basis consists of products of potential-optimized basis functions in the radial coordinates $R_{\mathrm{CaCl-H}}$ and $r_{\mathrm{Cl-Ca}}$, associated with Legendre functions in the angle γ, and Wigner rotation functions for the overall rotation of the complex. The radial basis functions are numerical eigenfunctions of one-dimensional Hamiltonians with potentials obtained from the three-dimensional global potential in the region of the insertion well by freezing the two other coordinates at their equilibrium values. A centrifugal sudden approximation is used, which decouples the calculations for different Ω values. This approximation is justified by the linear structure of the HCaCl insertion complex, which makes Ω a good quantum number. Bound states were calculated for $|\Omega|=0$, 1, and 2. A large basis of 16 800 functions, consisting of 50 Legendre functions in γ, 21 functions in R, and 16 functions in r, is used for each J,Ω. A nonorthogonal Lanczos iterative method[61] is used for the diagonalization.

The vibrational levels obtained from these calculations can be represented fairly well by the usual linear triatomic molecule expression

$$E(v_r,v_R,v_b) = \omega_r\left(v_r+\tfrac{1}{2}\right)+\omega_R\left(v_R+\tfrac{1}{2}\right)+\omega_b(v_b+1), \quad (8)$$

where ω_r and ω_R are the fundamental frequencies of the Ca–Cl and H–CaCl stretch vibrations, respectively, and ω_b is the fundamental bend frequency. The symbols v_r,v_R,v_b are the corresponding quantum numbers; Ω runs from $-v_b$ to v_b in steps of 2 and $J\geqslant|\Omega|$. The results are $\omega_r=355$ cm^{-1}, $\omega_R=1268$ cm^{-1}, and $\omega_b=127$ cm^{-1}, in good agreement with the results of the wave-packet calculations. The ground-state rotational constant B was extracted from the progression of the lowest levels for $J=0$, 1, etc. Off-diagonal Coriolis coupling had to be included in order to obtain a realistic value of B.

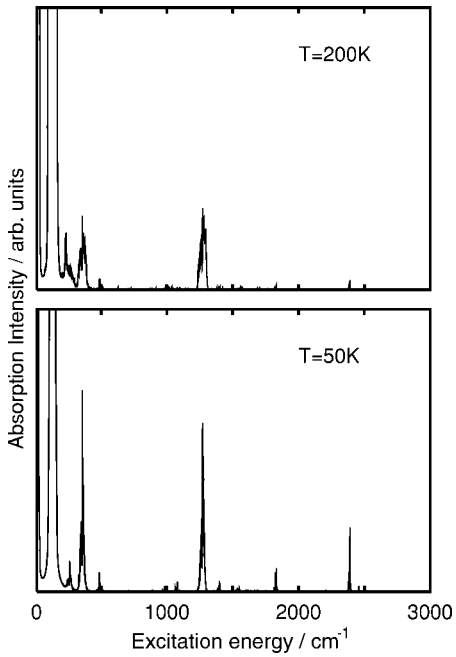

FIG. 9. Absorption spectrum of the HCaCl complex for different temperatures T. Homogeneous broadening parameter $\Gamma=1$ cm^{-1}.

The value of $B=0.13$ cm^{-1} is close to that computed from the equilibrium geometry.

The details of the calculation of the line strengths are given in Ref. 14. Absorption intensities are computed from these line strengths by averaging over a Boltzmann distribution of initial states. Figure 9 shows the absorption spectrum simulated at different temperatures, with the assumption that the lines are homogeneously broadened by Lorentzian functions of half-width at half maximum $\Gamma=1$ cm^{-1}. They agree nicely with the $T=0$ spectrum in Fig. 8. Detection of this spectrum will provide a check on the accuracy of our computed potential surface in the region of the insertion well.

VI. CONCLUSION

We reported the global potential-energy surface of the CaHCl system, describing the full reaction from $Ca(4s^2, {}^1S)+HCl$ reactants to $CaCl(X\,{}^2\Sigma)+H$ products. This surface is based on accurate *ab initio* calculations at the MRCI level. The reaction is endothermic by approximately 5100 cm^{-1}. There is a barrier of 4470 cm^{-1}, arising from an ionic/covalent crossing typical in harpoonlike reactions. The transition state complex has a bent geometry. On each side of this barrier is a well, a shallow van der Waals well in the Ca+HCl entrance channel, and a deep well corresponding to a HCaCl insertion complex. Both the van der Waals complex and the insertion complex have linear geometries.

Since the van der Waals well is important but is almost two orders of magnitude less deep than the insertion well, much attention was paid to the accurate computation of this shallow well. Detailed CCSD(T) calculations showed that the MRCI result for the van der Waals binding energy, $\approx$190 cm^{-1}, is underestimated by about 40 cm^{-1} ($\approx$30 cm^{-1} with respect to the CP corrected result). From a calculation of the bound vibrational states in the van der Waals well of the CCSD(T) and MRCI potentials it follows that the dissociation energies D_0 differ by about 20 cm^{-1}. A previous empirical estimate of the entrance channel well by de Castro–Vítores *et al.*[23] yielded a much higher binding energy, of $\approx$980 cm^{-1}, comprising a van der Waals contribution of $\approx$200 cm^{-1}, and a charge-transfer contribution of $\approx$800 cm^{-1}. The large charge-transfer term was probably introduced to explain the extraordinarily large binding energy of $\approx 1200\pm400$ cm^{-1} estimated by Menéndez *et al.*[55] The latter estimate used experimental photodissociation data with the assumption that the recoil energy of the products could be neglected. The much smaller binding energy from our calculations shows that this assumption must be reconsidered.

Also, the electric dipole moment function of this system was calculated. It provides valuable information about the changes in the charge distribution along the reaction path. The sudden increase of the dipole moment near the (rather late) transition state is due to a harpooning effect, and is related to an avoided crossing between covalent and ionic potentials. The dipole moment becomes much smaller at the deep insertion well; this can be explained by a near cancellation of two oppositely directed dipoles in the $H^-Ca^{++}Cl^-$ insertion complex. Finally, the dipole increases again to reach the value of the CaCl product, which has an ionic $Ca^{++}Cl^-$ core with a diffuse outer electron.

The electric dipole function was also calculated in the regions around the insertion and van der Waals wells and fitted to analytical forms. It was found that a simple point-charge model with nearly constant atomic charges nicely reproduces the dipole function in the region of the insertion well. This model confirms the $H^-Ca^{++}Cl^-$ ionic picture of the insertion complex.

Finally, rovibrational states were calculated in the insertion well and the infrared-absorption spectrum of the HCaCl insertion complex was simulated, with the goal to facilitate the experimental detection of this complex and establish the accuracy of our potential-energy surface. Further work on the dynamics of the $Ca+HCl\rightarrow CaCl+H$ reaction on the electronic ground- (X) state potential-energy surface is in progress.[62]

ACKNOWLEDGMENTS

We thank A. Aguado and M. Paniagua for interesting discussions, for providing us with their programs, and for advice on the fitting procedures. We thank P.E.S. Wormer for critically reading the manuscript. This work has been supported by MCYT(Spain), under Grant No. BFM2001-2179, and by the European Research Training Network THEONET II.

[1] J.-M. Mestdagh, B. Soep, M.-A. Gaveu, and J.-P. Visitcot, Int. Rev. Phys. Chem. **22**, 285 (2003).
[2] D. R. Herschbach, Adv. Chem. Phys. **10**, 319 (1966).
[3] M. Shapiro and Y. Zeiri, J. Chem. Phys. **70**, 5264 (1979).
[4] M. Baer, I. Last, and H. J. Loesch, J. Chem. Phys. **101**, 9648 (1994).
[5] G. A. Parker, A. Laganà, S. Crocchianti, and R. T Pack, J. Chem. Phys. **102**, 1238 (1995).
[6] F. Gögtas, G. G. Balint-Kurti, and A. R. Offer, J. Chem. Phys. **104**, 7927 (1996).

[7]A. Aguado, C. Tablero, and M. Paniagua, Comput. Phys. Commun. **108**, 259 (1998).
[8]A. W. Jasper, M. D. Hack, D. G. Truhlar, and P. Piecuch, J. Chem. Phys. **116**, 8353 (2002).
[9]X. Y. Chang, R. Ehlich, A. J. Hudson, P. Piecuch, and J. C. Polanyi, Faraday Discuss. **108**, 411 (1997).
[10]A. J. Hudson, H. B. Oh, J. C. Polanyi, and P. Piecuch, J. Chem. Phys. **113**, 9897 (2000).
[11]M. S. Topaler, D. G. Truhlar, X. Y. Chang, P. Piecuch, and J. C. Polanyi, J. Chem. Phys. **108**, 5349 (1998).
[12]M. S. Topaler, D. G. Truhlar, X. Y. Chang, P. Piecuch, and J. C. Polanyi, J. Chem. Phys. **108**, 5378 (1998).
[13]C. Sanz, O. Roncero, M. Paniagua, and A. Aguado, Chem. Phys. Lett. **351**, 295 (2002).
[14]A. Aguado, M. Paniagua, C. Sanz, and O. Roncero, J. Chem. Phys. **119**, 10088 (2003).
[15]A. Aguado, M. Lara, M. Paniagua, and O. Roncero, J. Chem. Phys. **114**, 3440 (2001).
[16]Y. Zeiri, G. Katz, R. Kosloff, M. S. Topaler, D. G. Truhlar, and J. C. Polanyi, Chem. Phys. Lett. **300**, 523 (1999).
[17]A. W. Jasper, M. D. Hack, A. Chakraborty, D. G. Truhlar, and P. Piecuch, J. Chem. Phys. **115**, 7945 (2001).
[18]U. Brinkmann and H. Telle, J. Phys. B **10**, 133 (1977).
[19]H. Telle and U. Brinkmann, Mol. Phys. **39**, 361 (1980).
[20]U. Brinkmann, V. H. Schmidt, and H. Telle, Chem. Phys. Lett. **73**, 530 (1980).
[21]C. T. Rettner and R. N. Zare, J. Chem. Phys. **75**, 3636 (1981).
[22]C. T. Rettner and R. N. Zare, J. Chem. Phys. **77**, 2416 (1982).
[23]M. de Castro-Vítores, R. Candori, F. Pirani, V. Aquilanti, M. Garay, and A. González-Ureña, Chem. Phys. Lett. **263**, 456 (1996).
[24]M. Garay, C. A. Rinaldi, J. M. Orea, and A. González-Ureña, Chem. Phys. Lett. **236**, 343 (1998).
[25]M. de Castro-Vítores, R. Candori, F. Pirani, V. Aquilanti, M. Garay, and A. González-Ureña, J. Phys. Chem. A **102**, 9537 (1998).
[26]M. Garay, J. M. Orea, A. González-Ureña, and G. Roberts, Mol. Phys. **97**, 967 (1999).
[27]A. J. H. M. Meijer, G. C. Groenenboom, and A. van der Avoird, J. Phys. Chem. A **101**, 7558 (1997).
[28]M. de Castro-Vítores, R. Candori, F. Pirani, V. Aquilanti, M. Garay, and A. González-Ureña, J. Chem. Phys. **112**, 770 (2000).
[29]B. Soep, C. J. Whitham, A. Keller, and J. P. Visticot, Faraday Discuss. Chem. Soc. **91**, 191 (1991).
[30]B. Soep, S. Abbés, A. Keller, and J. P. Visticot, J. Chem. Phys. **96**, 440 (1992).
[31]A. Keller, R. Lawruszczuk, B. Soep, and J. P. Visticot, J. Chem. Phys. **105**, 4556 (1996).
[32]R. Lawruszczuk, M. Elhanine, and B. Soep, J. Chem. Phys. **108**, 8374 (1998).
[33]M.-L. Dubernet and J. Hutson, J. Chem. Phys. **101**, 1939 (1994).
[34]A. D. Isaacson and J. T. Muckerman, J. Chem. Phys. **73**, 1729 (1980).
[35]R. L. Jaffe, M. D. Pattengill, F. G. Mascarello, and R. N. Zare, J. Chem. Phys. **86**, 6150 (1987).
[36]V. Sanz, A. Aguado, and M. Paniagua, J. Mol. Struct.: THEOCHEM **426**, 165 (1998).
[37]M.-Q. Cai, L. Zhang, B.-Y. Tang, M.-D. Chen, G.-W. Yang, and K.-L. Han, Chem. Phys. **255**, 283 (2000).
[38]M. J. McGuire, P. Piecuch, K. Kowalski, S. A. Kucharski, and M. Musia, J. Phys. Chem. A **108**, 8878 (2004).
[39]H.-J. Werner, P. J. Knowles, J. Almlöf *et al.*, MOLPRO (Version 2002.7).
[40]T. Leininger and G. H. Jeung, J. Chem. Phys. **103**, 3942 (1995).
[41]A. J. H. Wachter, J. Chem. Phys. **52**, 1033 (1970).
[42]A. J. H. M. Meijer, G. C. Groenenboom, and A. van der Avoird, J. Chem. Phys. **101**, 7603 (1994).
[43]T. H. Dunning, Jr., J. Chem. Phys. **90**, 1007 (1989).
[44]D. E. Woon and T. H. Dunning, Jr., J. Chem. Phys. **98**, 1358 (1993).
[45]J. E. Hansen, C. Laughlin, H. W. van der Hart, and G. Verbockhaven, J. Phys. B **32**, 2099 (1999).
[46]S. R. Langhoff and E. R. Davidson, Int. J. Quantum Chem. **8**, 61 (1974).
[47]S. F. Boys and F. Bernardi, Mol. Phys. **19**, 553 (1970).
[48]K. P. Huber and G. Herzberg, *Constant and Diatomic Molecules* (Van Nostrand Reinhold, New York, 1979).
[49]A. Aguado and M. Paniagua, J. Chem. Phys. **96**, 1265 (1992).
[50]A. Aguado private communication.
[51]C. Sanz, Master thesis, Universidad Autonoma de Madrid, 2000.
[52]A. Aguado, O. Roncero, C. Tablero, C. Sanz, and M. Paniagua, J. Chem. Phys. **112**, 1240 (2000).
[53]A. Aguado, M. Paniagua, M. Lara, and O. Roncero, J. Chem. Phys. **107**, 10085 (1997).
[54]J. A. Shea and E. J. Campbell, J. Chem. Phys. **81**, 5326 (1984).
[55]M. Menéndez, M. Garay, E. Verdasco, and A. González-Ureña, J. Chem. Soc., Faraday Trans. **89**, 1493 (1993).
[56]G. C. Groenenboom and I. M. Struniewicz, J. Chem. Phys. **113**, 9562 (2000).
[57]B. T. Sutcliffe and J. Tennyson, Int. J. Quantum Chem. **39**, 183 (1991).
[58]S. F. Rice, H. Martin, and R. W. Field, J. Chem. Phys. **82**, 5023 (1985).
[59]S. Raouafi, G.-H. Jeung, and Ch. Jungen, J. Chem. Phys. **115**, 7450 (2001).
[60]M. Paniagua, A. Aguado, M. Lara, and O. Roncero, J. Chem. Phys. **111**, 6712 (1999).
[61]J. K. Cullum and R. A. Willoughby, *Lanczos Algorithms for Large Symmetric Eigenvalues Computations* (Birkhäuser, Boston, 1985).
[62]C. Sanz, A. van der Avoird, and O. Roncero, in preparation.
[63]J. Sugar and C. J. Corliss, J. Phys. Chem. Ref. Data **14**, Suppl. 2 (1985).
[64]F. M. Kelly and M. S. Mathur, Can. J. Phys. **58**, 1004 (1980).
[65]F. M. Kelly and M. S. Mathur, Can. J. Phys. **58**, 1418 (1980).
[66]L. P. Lellouch and L. R. Hunter, Phys. Rev. A **36**, 3490 (1987).
[67]H. Martin, J. Chem. Phys. **88**, 1797 (1987).
[68]J. A. Coxon and P. G. Hajigeorgiou, J. Mol. Spectrosc. **203**, 49 (2000).